Journal of Marine Research, 51, 843–868, 1993

Coupled effects of vertical mixing and benthic grazing on phytoplankton populations in shallow, turbid estuaries

by **Jeffrey R. Koseff**[1], **Jacqueline K. Holen**[1], **Stephen G. Monismith**[1] and **James E. Cloern**[2]

ABSTRACT

Coastal ocean waters tend to have very different patterns of phytoplankton biomass variability from the open ocean, and the connections between physical variability and phytoplankton bloom dynamics are less well established for these shallow systems. Predictions of biological responses to physical variability in these environments is inherently difficult because the recurrent seasonal patterns of mixing are complicated by aperiodic fluctuations in river discharge and the high-frequency components of tidal variability. We might expect, then, less predictable and more complex bloom dynamics in these shallow coastal systems compared with the open ocean. Given this complex and dynamic physical environment, can we develop a quantitative framework to define the physical regimes necessary for bloom inception, and can we identify the important mechanisms of physical-biological coupling that lead to the initiation and termination of blooms in estuaries and shallow coastal waters? Numerical modeling provides one approach to address these questions. Here we present results of simulation experiments with a refined version of Cloern's (1991) model in which mixing processes are treated more realistically to reflect the dynamic nature of turbulence generation in estuaries. We investigated several simple models for the turbulent mixing coefficient. We found that the addition of diurnal tidal variation to Cloern's model greatly reduces biomass growth indicating that variations of mixing on the time scale of hours are crucial. Furthermore, we found that for conditions representative of South San Francisco Bay, numerical simulations only allowed for bloom development when the water column was stratified and when minimal mixing was prescribed in the upper layer. Stratification, however, itself is *not* sufficient to ensure that a bloom will develop: minimal wind stirring is a further prerequisite to bloom development in shallow turbid estuaries with abundant populations of benthic suspension feeders.

1. Introduction

Phytoplankton populations are dynamic; the prominent annual feature of biomass change in the open ocean is the spring bloom, which has been a focus of research since the beginnings of biological oceanography. Phytoplankton blooms occur when the rate of primary production temporarily exceeds the cumulative rates of all

1. Environmental Fluid Mechanics Laboratory, Department of Civil Engineering, Stanford University, Stanford, California 94305-4020, U.S.A.
2. U.S. Geological Survey, MS496, 345 Middlefield Road, Menlo Park, California, 94025, U.S.A.

biomass losses; hence, they are departures from population 'quasi-equilibrium' (Evans and Parslow, 1985). A rich history of observation and theory has established firmly the physical basis for oceanic spring blooms, which accompany seasonal changes in the depth of the upper mixed layer. Following earlier works by Gran and Braarud (1935), Riley (1942), and Sverdrup (1953), Platt *et al.* (1991) conclude that: "Incipient stabilization of the water column by surface heating can then be seen as the fundamental process that promotes the rapid growth of phytoplankton that leads to the incidence of a bloom." Rapid population growth at bloom inception is a direct result of the increased light exposure to algal cells in the upper mixed layer once the seasonal thermocline develops. For the deep ocean, numerical models describe well the spatial and temporal evolution of the spring bloom (e.g. in the North Atlantic; Wroblewski, 1989), and a quantitative framework exists to define the physical regime necessary for bloom inception (Platt *et al.,* 1991).

Shallow shelf waters and estuaries have very different physical regimes from the open ocean, and the connections between physical variability and phytoplankton bloom dynamics are less well established for these systems. Furthermore, the coastal ocean waters tend to have very different patterns of phytoplankton biomass variability. For example, winter blooms of diatoms (Hitchcock and Smayda, 1977) or dinoflagellates (Sellner *et al.,* 1991) are recurrent seasonal events in some estuaries. Large, episodic blooms dominated by one or several taxa, including toxic species, are global occurrences in coastal waters (Smayda, 1989). Finally, seasonal fluctuations in phytoplankton biomass can be difficult to resolve in coastal waters where high-frequency variability is observed over periods of hours (Fortier and Legendre, 1979) to days (Sinclair *et al.,* 1981). These varied patterns of phytoplankton biomass fluctuation might result, in part, from the unique physical regime of coastal ecosystems where (1) the water depth is shallow, and (2) the physical and chemical environments are strongly influenced by river runoff. For example, Simpson *et al.* (1990; 1991) have explored the complex nature of vertical mixing in coastal regions under freshwater influence, where density structure is highly dynamic and controlled by the balance between buoyancy inputs from surface heating plus freshwater and stirring from tidal plus wind stresses. Predictions of biological responses to physical variability in these environments are inherently difficult because the recurrent seasonal patterns of mixing are complicated by aperiodic fluctuations in river discharge and the high-frequency components of tidal variability (Simpson *et al.,* 1991). We might expect, then, less predictable and more complex bloom dynamics in these shallow coastal systems compared with the open ocean.

Other distinctions between the physical regimes of the deep and coastal ocean directly influence the observed differences in phytoplankton dynamics in the coastal systems. Shallow coastal waters have high concentrations of suspended particulate matter (SPM) that originate from wind-wave or tidal resuspension of bed sediments as well as riverine inputs of terrigenous SPM. Consequently, coastal ecosystems are

characterized by large spatial variability of turbidity (e.g. Gieskes and Kraay, 1975) and temporal variability from hours to seasons (e.g. Cloern *et al.,* 1989). Light attenuation by SPM acts as a major control on phytoplankton photosynthesis (and population growth rate) in shallow marine systems (e.g., Colijn, 1982), so much of the spatial and temporal variability of phytoplankton primary production is associated with variability in SPM concentration (Cloern, 1987). However, nutrient availability is relatively high in coastal waters because of terrigenous inputs (e.g. Malone, 1992) as well as rapid rates of recycling, both in the water column and benthos (Nixon, 1981; Kemp and Boynton, 1984). Finally, the benthos can act as an important sink for phytoplankton biomass through consumption by macrofaunal suspension feeders. Much of the primary production in some shallow marine systems is apparently consumed by the benthos (e.g. Cloern, 1982), and this process of benthic-pelagic coupling can be a control mechanism of phytoplankton population variability in estuaries.

Given this complex and dynamic physical environment, can we develop a quantitative framework to define the physical regimes necessary for bloom inception, and can we identify the important mechanisms of physical-biological coupling that lead to the initiation and termination of blooms in estuaries and shallow coastal waters? Numerical modeling provides one approach to address these questions. For example, Cloern (1991) used simulation experiments with a simple 1-D vertical model to suggest how phytoplankton bloom dynamics in shallow estuaries, such as South San Francisco Bay, might be controlled by daily fluctuations in the intensity of tidal stirring. (Cloern used a sinusoidal variation over a period of 14 days as a first-order approximation to the spring-neap tidal cycle, hereafter referred to as M_{sn}.) However, that model incorporated a rudimentary treatment of the complex mixing processes in estuaries and did not include, for example, vertical variability in turbulent mixing intensity, effects of density stratification, wind stirring, or high-frequency components of variability associated with the semidiurnal (M_2) tides. Here we present results of simulation experiments with a refined version of Cloern's (1991) model in which mixing processes are treated more realistically to reflect the dynamic nature of turbulence generation in estuaries. These differences are described more fully in Section 3. The numerical experiments described here were motivated by three specific questions:

Q1: *In shallow coastal systems, what combinations of coupled physical-biological processes are necessary for phytoplankton biomass increase—i.e., can we make generalizations about the sets of conditions that are necessary for bloom initiation? What are the controlling parameters?*

Q2: *Are simulation results fundamentally different when turbulent mixing is treated as a spatially-variable process that reflects (a) the importance of both tidal stress at the bed and wind stress at the surface, and (b) effects of salinity (density) stratification on the vertical distribution of turbulence?*

Table 1. Description of variables.

Name	Value	Units	Description
z		m	Depth
t		d	Time
$B(z, t)$		mg m^{-3}	Phytoplankton biomass (chl *a*)
$\mu(z, t)$		d^{-1}	Phytoplankton growth rate
K		$m^2\ d^{-1}$	Turbulent mixing coefficient
α	8	$m^3\ m^{-2}\ d^{-1}$	Benthic grazing rate
w_s	0.5	m d^{-1}	Phytoplankton sinking rate
H	10	m	Water column height
r_1	0.05		Phytoplankton respiration rate as percentage of Pmax
G	0.1	d^{-1}	Zooplankton grazing rate
$I(z, t)$		Einst. $m^{-2}\ d^{-1}$	Solar radiation
$I(0)$	40	Einst. $m^{-2}\ d^{-1}$	Mean daily incident solar radiation
k	1.3	m^{-1}	Light attenuation coefficient
$P(z, t)$		mg C mg^{-1} chl *a* d^{-1}	Biomass-specific rate of photosynthesis
P_{max}	100	mg C mg^{-1} chl *a* d^{-1}	Light-saturation rate of photosynthesis
u_{avg}	.5	m s^{-1}	Average flow velocity

Q3: *Are simulation results sensitive to the frequencies of physical variability included in coupled physical-biological models? In particular, Cloern (1991), Winter et al. (1975), and others have specified a mean daily rate of vertical mixing. However, the rate of turbulent mixing is a continuous function of time; is the high-frequency (M_2) variability in mixing intensity critical to the details of bloom evolution?*

We begin with a scaling analysis of the model used by Cloern to address Question 1. Then we present refinements of the constructs used to simulate vertical mixing, and use results from this more realistic numerical model to address Questions 2 and 3. Our emphasis here is on spatial and high-frequency variability in mixing processes; short-term fluctuations in biological processes (e.g. photosynthetic efficiency) may also be important (e.g. Fortier and Legendre, 1979).

2. Nondimensional analysis of the simple 1-d model

a. The general model. As presented in Cloern (1991), phytoplankton biomass measured as chlorophyll *a* is modeled by a one-dimensional advection-diffusion equation. The model includes biomass production, losses to respiration and zooplankton grazing in the water column and benthic grazing at the bed, and transport (vertical only) due to sinking and turbulent mixing (referred to as eddy diffusivity in Cloern, 1991) in the water column. With the variables described in Table 1, the governing

equation relating the variation of phytoplankton biomass B is

$$\frac{\partial B}{\partial t} = \mu_{net}B + \frac{\partial}{\partial z}\left(K\frac{\partial B}{\partial z}\right) - \frac{\partial}{\partial z}(w_sB) \tag{1}$$

where $\partial/\partial z(w_sB)$ is the gradient of the advective flux of biomass due to sinking, $\partial/\partial z(K\,(\partial B/\partial z)$ is the gradient of the diffusive transport due to turbulent mixing, and μ_{net} is the net biomass-specific rate of population growth including losses to respiration and zooplankton grazing (G),

$$\mu_{net} = \mu - G. \tag{2}$$

We consider a water column of 10 m depth in which the net compensation depth, the depth at which $\mu_{net} = 0$, is 3 m (a condition typical of South San Francisco Bay in spring). Thus the top 3 m of the water column is a net source of biomass, and the bottom 7 m are a net sink. At the surface there is a no flux boundary condition

$$-w_sB + K\frac{\partial B}{\partial z} = 0 \qquad (z = 0), \tag{3}$$

and at the bottom boundary the flux of biomass due to sinking and mixing equals the flux due to benthic grazing parameterized as a community filtration rate α

$$-w_sB + K\frac{\partial B}{\partial z} = -\alpha B \qquad (z = H). \tag{4}$$

In the model, the phytoplankton sinking rate, w_s, and the benthic grazing rate, α, are constants, and, as explained below, we investigated a range of values of both w_s and α. For spring conditions in South San Francisco Bay, Cloern (1991) specified a sinking rate of 0.5 m d^{-1} and a benthic grazing rate of 8 m^3 m^{-2} d^{-1}.

b. The phytoplankton production model. The phytoplankton production model is based on the photosynthesis-irradiance equation of Jassby and Platt (1976). The growth rate μ is computed as a function of depth from the productivity P described by:

$$P(z, t) = P_{max}\{\tanh\,[aI(z)] - r_1\}, \tag{5}$$

where $a = 0.1$ defines photosynthetic efficiency at low irradiance, $r_1 = 0.05$ is the respiration loss rate (5% of the maximum rate of photosynthesis), and all other variables (following Cloern, 1991) are defined in Table 1.

The depth-distribution of photosynthetically-active solar irradiance, $I(z)$, is calculated from

$$I(z) = I(0)\exp\,[-(k + k_sB(1, t))z], \tag{6}$$

where $I(0)$ is mean daily incident solar radiation; k is the mean light attenuation coefficient from abiotic sources of light absorption and scattering; k_s is the component of light attenuation from phytoplankton biomass taken as 0.016 m^2 mg^{-1} chlorophyll *a* (Bannister, 1974), and $B(1, t)$ is the biomass at a depth of 1 m.

Finally, the specific growth rate can be determined from productivity by assuming that the ratio θ of phytoplankton cellular carbon to chlorophyll *a* is a constant equal to 50 (Wienke and Cloern, 1987) from

$$\mu(z, t) = P(z, t)/\theta. \tag{7}$$

Values for all parameters were chosen to represent spring conditions in South San Francisco Bay (Cole and Cloern 1984; 1987). The simulations began with a uniform biomass distribution, $B(z, t = 0) = B_0$, where B_0 is a constant. As explained in Section 2d, the governing equations do not depend on the value of B_0; the results simply scale according to the initial biomass distribution. Thus, it is convenient to choose B_0 = 1.0 mg m^{-3} chlorophyll *a*. The baseline level of mean chlorophyll *a* observed in South San Francisco Bay is about 2.0–3.0 mg m^{-3}.

c. Scaling. To understand the roles of the various source and physical transport terms in the problem, we performed a fractional analysis (e.g., Lyne, 1983) to identify the important parameter ratios. For this part of the analysis we assume that the sinking rate w_s and the benthic grazing rate α are constant. We define the nondimensional parameters $B^*(z, t), z^*, t^*, K^*(z, t)$, and $\mu^*_{net}(z, t)$ by

$$B = B_0 B^* \tag{8}$$

$$t = \tau t^* \tag{9}$$

$$z = H z^* \tag{10}$$

$$K = \epsilon K^* \tag{11}$$

$$\mu_{net} = \overline{\mu_{net}} \mu^*_{net}. \tag{12}$$

B_0, τ, H, ϵ, $\overline{\mu_{net}}$ are constants: B_0 is the initial depth-averaged biomass, H is the depth of the water column, ϵ is a characteristic value of the turbulent mixing, $\overline{\mu_{net}}$ is the depth-averaged rate of phytoplankton growth at $t = 0$,

$$\overline{\mu_{net}} = \frac{1}{H} \int_0^H \mu_{net}(z, 0)\, dz \tag{13}$$

and we choose τ to be the time scale of phytoplankton production,

$$\tau = \tau_{prod} = \frac{1}{\overline{\mu_{net}}}. \tag{14}$$

The other nondimensional time scales of Eqs. (1), (3), and (4) are those of phytoplankton diffusion, sinking, and grazing respectively:

$$\tau_{\text{diff}} = H^2/K \tag{15}$$

$$\tau_{\text{sink}} = H/w_s \tag{16}$$

$$\tau_{\text{graze}} = H/\alpha. \tag{17}$$

τ_{diff} is the approximate time it takes for the turbulence in the water column (characterized by K) to mix the biomass over the water column of depth H; τ_{sink} is the approximate time that it would take a phytoplankton cell to sink at a rate w_s over the depth H; and τ_{graze} is the approximate time it would take to deplete a water column of depth H of biomass if benthic consumption were occurring at rate α.

Substituting the relations (8)–(12) and (14) into Eqs. (1), (3) and (4) yields the nondimensional form of the governing equations:

$$\frac{\partial B^*}{\partial t^*} = \mu^*_{\text{net}} B^* + \left(\frac{\epsilon}{\overline{\mu_{\text{net}}} H^2}\right)\frac{\partial}{\partial z}\left(K^* \frac{\partial B^*}{\partial z^*}\right) - \left(\frac{w_s}{\overline{\mu_{\text{net}}} H}\right)\frac{\partial B^*}{\partial z^*} \tag{18}$$

$$-\left(\frac{w_s}{\overline{\mu_{\text{net}}} H}\right)B^* + \left(\frac{\epsilon}{\overline{\mu_{\text{net}}} H^2}\right)K^* \frac{\partial B^*}{\partial z^*} = 0 \qquad (z^* = 0) \tag{19}$$

$$-\left(\frac{w_s}{\overline{\mu_{\text{net}}} H}\right)B^* + \left(\frac{\alpha}{\overline{\mu_{\text{net}}} H}\right)B^* + \left(\frac{\epsilon}{\overline{\mu_{\text{net}}} H^2}\right)K^* \frac{\partial B^*}{\partial z^*} = 0 \qquad (z^* = 1) \tag{20}$$

Eqs. (18) through (20) do not include the initial depth-averaged biomass B_0, which cancels out. Hence, the behavior of the system does not depend on the magnitude of the initial biomass. Eqs. (18) through (20) show that the solution depends on three nondimensional parameters

$$K' = \frac{\epsilon}{\overline{\mu_{\text{net}}} H^2} = \frac{\tau_{\text{prod}}}{\tau_{\text{diff}}} \tag{21}$$

$$w'_s = \frac{w_s}{\overline{\mu_{\text{net}}} H} = \frac{\tau_{\text{prod}}}{\tau_{\text{sin}\,k}} \tag{22}$$

$$\alpha' = \frac{\alpha}{\overline{\mu_{\text{net}}} H} = \frac{\tau_{\text{prod}}}{\tau_{\text{graze}}} \tag{23}$$

which are the ratios of the time scales of production:diffusion, production:sinking, and production:grazing, respectively.

The above analysis identifies three important time scales (and time scale ratios) in our formulation of the problem. We have implicitly assumed that the physiological time scales are much longer than the physical time scales, i.e., physiological changes

occur slowly compared to physical changes, and we have ignored them in our analysis (we discuss this assumption in Section 5). By comparing the ratios of the physical time scales we can determine under what general conditions phytoplankton biomass is likely to increase (bloom) and under what conditions it will decrease (decay). For example, if K' is large (diffusion time scale shorter than the production time scale) a surface bloom is unlikely because the phytoplankton will be mixed over the water column depth in a much shorter time than it can be produced in the euphotic zone, thereby enhancing the losses to aphotic zone respiration and benthic grazing. Similarly, if α' is large (grazing time scale much shorter than the production time scale) a bloom is unlikely because grazing at the bed would occur much faster than phytoplankton production, thereby minimizing phytoplankton biomass at the bottom boundary.

We can formalize this analysis and illustrate it analytically by integrating equation (18) over depth and time. Letting $\overline{B}(t^*)$ be the nondimensional depth-averaged biomass at time t^*,

$$\overline{B}(t^*) = \int_0^1 B^*(z^*, t^*)dz^*, \tag{24}$$

and using boundary conditions (19) and (20), integration over depth of Eq. (18) yields an evolution equation for the nondimensional depth-integrated biomass:

$$\begin{aligned} \frac{\partial \overline{B}(t^*)}{\partial t^*} &= \int_0^1 \mu^*_{\text{net}} B^*\, dz^* - \left(\frac{\alpha}{\overline{\mu_{\text{net}}} H}\right) B^*(z^* = 1) \\ &= \overline{B} \int_0^1 \mu^*_{\text{net}} \frac{B^*}{\overline{B}}\, dz^* - \left(\frac{\alpha \overline{B}}{\overline{\mu_{\text{net}}} H}\right) \frac{B^*(z^* = 1)}{\overline{B}} \end{aligned} \tag{25}$$

where B^* and μ^*_{net} are functions of t^* and z^*, and $\overline{B}$ is a function of t^*. If the rate of phytoplankton mixing is rapid compared to its production and sinking rates (i.e. if $\tau_{\text{diff}} \ll \tau_{\text{prod}}$ and τ_{sink}), then the biomass will be essentially uniformly distributed in depth. This means that $B^*(1, t^*) \approx B^*(z^*, t^*) \approx \overline{B}(t^*)$, so using

$$\int_0^1 \mu^*_{\text{net}}(z^*, t^*)\, dz^* = 1,$$

Eq. (25) simplifies to

$$\frac{\partial \overline{B}(t^*)}{\partial t^*} = \left(1 - \frac{\alpha}{\overline{\mu_{\text{net}}} H}\right) \overline{B}(t^*)$$

or

$$\overline{B}(t^*) = \overline{B}(t^* = 0) \exp\left[(1 - \alpha')t^*\right]. \tag{26}$$

Eq. (26) shows that given the assumption of rapid mixing, whenever benthic grazing

is weak ($\tau_{graze} > \tau_{prod}$; $\alpha' < 1$) then the depth averaged biomass increases exponentially, i.e. a bloom can occur. If, however, the grazing is rapid ($\tau_{graze} < \tau_{prod}$; $\alpha' > 1$) then $\bar{B}$ decreases exponentially, i.e. a bloom is not possible. Therefore, in water columns actively mixed by turbulence, a bloom can only occur if the benthic grazing pressure is relatively weak.

If, however, mixing is slow, then gradients in concentration induced near the bed by benthic grazing will not be mixed out and a concentration boundary layer will form so that $B^*(z^* = 1) < \bar{B}$, and

$$\int_0^1 \mu^*_{net} \frac{B^*}{\bar{B}} dz^* > 1.$$

Hence, the critical value of benthic grazing rate required to suppress biomass increase in slower mixing conditions is larger than that in rapid mixing conditions. This means that blooms are more likely to occur in water columns where mixing is less vigorous or, if the water column is stratified, above the parts of the water column where the stratification suppresses the mixing (see Section 3a). In addition, this analysis shows that hydrodynamic processes can directly affect the strength of benthic-pelagic coupling, and it illustrates the importance of the time variance in the mixing model. These issues will be discussed in more detail in Section 3.

d. The numerical model. The numerical model uses the Crank-Nicolson finite difference method to discretize the governing equations (1), (3), and (4). Because these equations are in conservative form, the numerical solution is effectively a finite volume scheme. This method is appropriate because the diffusion term in equation (1) generally dominates the transport for the range of parameters used here. This scheme is second order accurate in time and space, and it does not introduce numerical diffusion. However, the solution scheme is extremely sensitive to very low values of the turbulent mixing coefficient K. Thus, the case of $K = 0$ is not permitted in our turbulent mixing models, and we add the factor K_0, taken to be 0.1 m^2d^{-1}, to our computed K in Eq. (28) (see Section 3c).

The Crank-Nicolson scheme involves central differences in the spatial coordinate, so the top and bottom boundaries require special treatment. To model the boundary conditions in a consistent and grid-independent fashion, we used phantom points above and below the upper and lower boundaries, respectively. We performed extensive numerical experiments to validate the discretization and grid independence of the numerical scheme as well as to confirm the mass conservation properties of the scheme.

The spatial discretization step used in all these simulations was 0.05 m, and the time step used was 0.0005 days. Based on the sinking velocity, w_s, the Courant number for these simulations varies from 0.005 to 0.03. The Crank-Nicolson scheme does not have a Courant number limitation for stability, but a very small time step

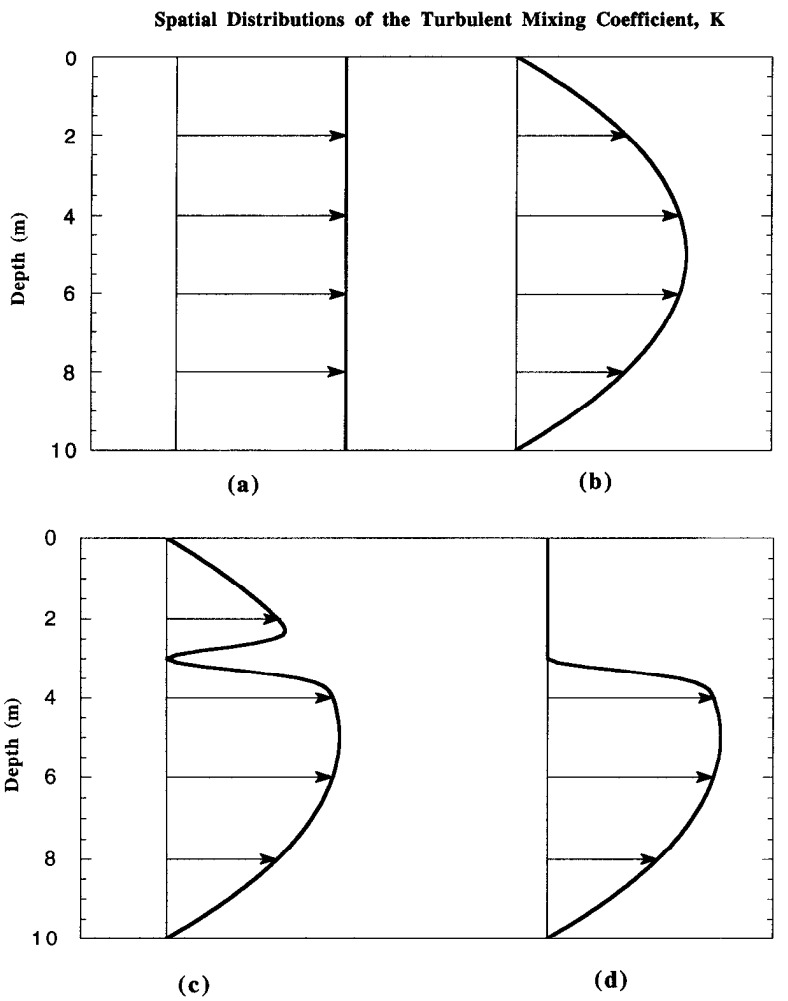

Figure 1. Schematic showing vertical distributions of the turbulent mixing coefficient K: (a) uniform distribution, (b) parabolic distribution, (c) parabolic with stratification function, and (d) parabolic with stratification and zero upper layer mixing.

was used to preserve the max-min property of the solution (see Greenspan and Casulli, 1988) especially in regions where the turbulent diffusivity is small and Eq. (1) becomes more hyperbolic in nature.

e. Numerical investigation of the nondimensional equations. To quantitatively investigate the relative effects of mixing and grazing on phytoplankton dynamics, we ran numerical tests with a range of values for the diffusion and grazing parameters of Eqs. (27) and (29), with several values of w_s, and with K constant in time and uniform in space (see Fig. 1a). These numerical tests show that regardless of the values of α'

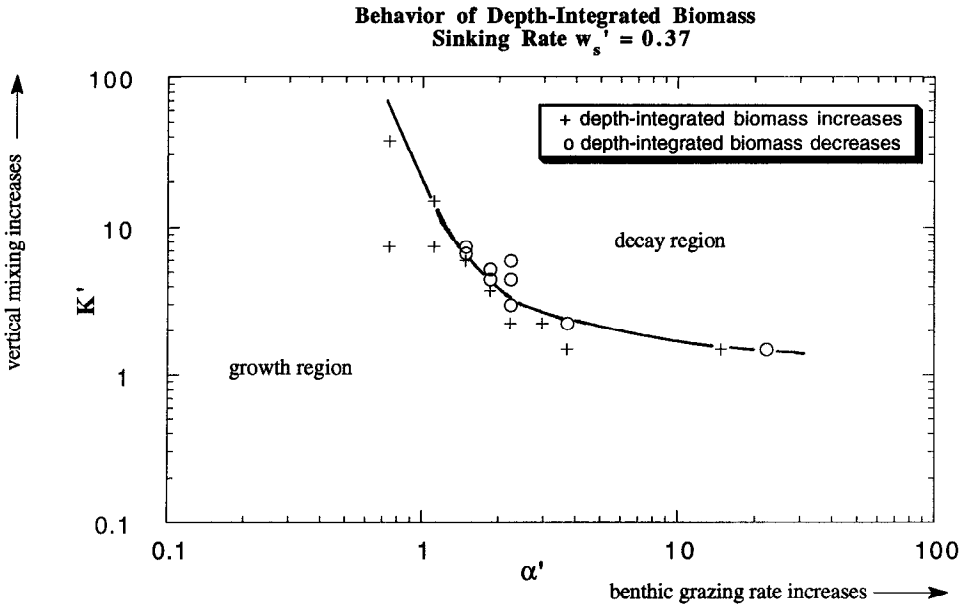

Figure 2. Behavior of depth-integrated biomass as a function of turbulent diffusivity and grazing strength at a fixed value of sinking rate. All variables are non-dimensionalized according to Eqs. (21) to (23), and turbulent diffusivity distribution is uniform (Fig. 1a). Curve is dividing line between the growth and decay regions.

and K' (but with K constant), after a possible initial transient (over less than one day), the integrated biomass $\overline{B}$ either increases or decreases monotonically.

Recall that our scaling arguments show that with the assumption of rapid mixing ($K' \gg 1$) then if $\alpha' < 1$ the depth averaged biomass $\overline{B}$ increases exponentially, indicating a bloom. If, however, grazing is rapid ($\alpha' > 1$) then $\overline{B}$ decreases exponentially, indicating a decay. The coupled effects of vertical mixing and benthic grazing are illustrated in Figure 2 which summarizes the results of our numerical simulations, and in particular the behavior of $\overline{B}$ for a range of points in the α'-K' plane for the case of w_s' = .37 (w_s = .5 m d^{-1}). The figure shows a separation of the α'-K' plane into distinct regions of biomass increase or decrease corresponding to the conditions defined by the scaling analysis. For example, when K' is 7.4 (corresponds in Eq. 21 to a characteristic value of turbulent diffusivity of ϵ = 100 m^2 d^{-1}), biomass will increase only when α' is less than 1.1, (α < 1.5 m^3 m^{-2} d^{-1}), and it will decay whenever α' is greater than 1.5, (α > 2.0 m^3 m^{-2} d^{-1}). For α' as low as 0.7 (α = 1.0 m^3 m^{-2} d^{-1}), a value of K' = 37 (ϵ = 500 m^2 d^{-1}) still results in a biomass increase. However, when α' is very large then the only way a bloom can form is if values of K' are very small, i.e. mixing is very slow. For example, when α' is as high as 22.2 (α = 30 m^3 m^{-2} d^{-1}), the biomass decays even with K' as low as 1.5 (ϵ = 20 m^2 d^{-1}). Although these results are

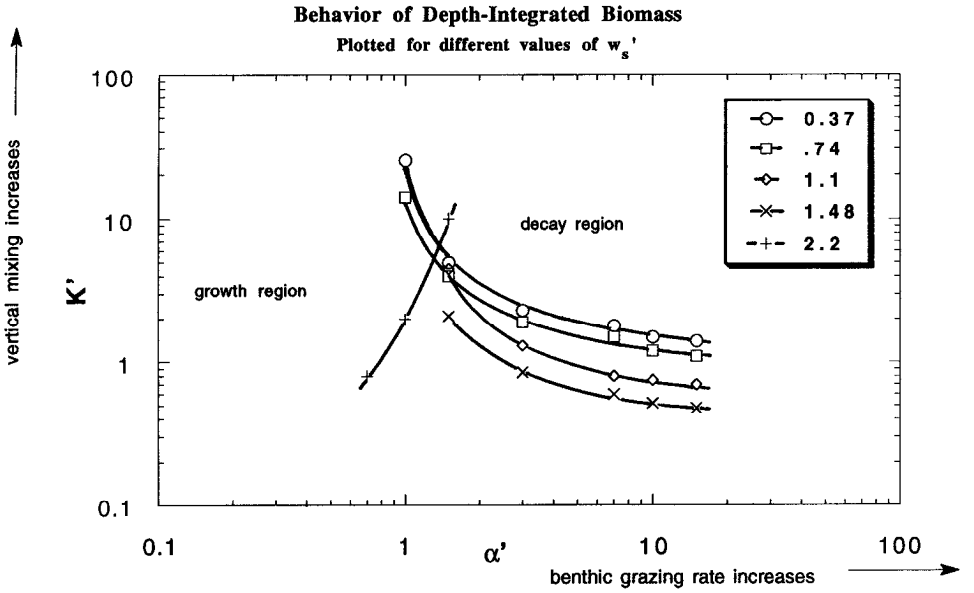

Figure 3. Behavior of depth-integrated biomass as a function of turbulent diffusivity and grazing strength for various values of sinking rate. All variables are non-dimensionalized according to Eqs. (21) to (23) and turbulent diffusivity distribution is uniform (Fig. 1a). The curves are the dividing lines between the growth and decay regions for each w_s'. In the case of $w_s' = 2.2$ (+) the growth region lies to the left of the curve.

for a highly simplified model of K, they indicate the type of behavior to expect from more complex turbulent mixing models.

The above results were all for a constant sinking rate w_s of .5 m d^{-1}. For comparison the results for four other sinking rates (1, 1.5, 2, and 3 m d^{-1}, corresponding to w_s' of 0.74, 1.1, 1.48, and 2.2 respectively) are shown in Figure 3. For increasing values of w_s' up to 1.48 the plot shows that for a given α' ($\alpha' > 3$) a progressively smaller K' is required to produce a biomass decay. Biomass increase can occur over a wide range of α' as long as K' is small. At w_s' of 2.2, however, the behavior is completely different and the results show that the growth region in the α'-K' domain is greatly reduced. This means that for sinking rates greater than 3 m d^{-1}, the only way for biomass to increase is under conditions of very mild mixing and very small benthic grazing.

Results in Figure 3 confirm that benthic grazing, vertical mixing, and sinking are all important in determining the sign of phytoplankton biomass change in shallow marine systems. The coupled effects of the three processes can be expressed as maps in α'-K'-w_s' space that define the separate regions of potential biomass increase and biomass decrease.

3. Steps toward physical realism

Cloern's model results demonstrated that phytoplankton population fluctuations can be sensitive to fluctuations in vertical mixing at the time scale of days (e.g., over spring-neap, M_{sn} cycle). However, the model did not incorporate spatial variability in K, the effects of density stratification and wind stirring, or the higher frequency components of variability associated with the semidiurnal (M_2) tides. Here we follow the results from Section 2 and describe an approach in which the spatial and temporal variability of turbulent mixing can be included in a more realistic model of coupled mixing, production, and grazing processes.

a. Vertical variation of K– *a simple model.* Turbulence in estuarine water columns is generated primarily by shear stresses at the surface by the wind and at the bottom by the tidal currents (Simpson *et al.,* 1990; 1991). In simple transport models, such as the one described here, the effect of the turbulence on mixing is typically parameterized by an eddy diffusivity (turbulent mixing coefficient), K. Following the arguments of Taylor (1954), the eddy diffusivity is characterized by a turbulent velocity scale and a length scale. In estuaries these parameters are typically the shear velocity u^* and the depth of the estuary H.

When there is only one primary source of turbulence, the vertical distribution of K is parabolic in shape with a maximum at mid-depth. For example, we can derive the vertical mixing coefficient for estuarine or riverine flow from the fluid velocity profile (Fischer *et al.,* 1979). Using the logarithmic law velocity profile, the vertical mixing coefficient for both momentum and mass transport becomes

$$K(z) = \kappa H u_* \left[\frac{z}{H}\right]\left[1 - \left(\frac{z}{H}\right)\right] \tag{27}$$

where $\kappa = 0.4$ is the von Karman constant and u_* is the shear velocity. The shear velocity is defined as $u_* = \sqrt{C_d} u_{avg}$, where C_d is the drag coefficient at the bottom (we use $C_d = .0015$), and u_{avg} is a velocity representative of the tidally induced free-stream velocity.

With both sources of turbulence, the distribution of K is likely to be given by a superposition of two parabolic distributions and will, therefore, be similar in shape but with higher values (see Fig. 1b). The parabolic distribution is not unique to the model formulation we have used for K in this paper; the same distribution is obtained using a Mellor-Yamada turbulence model (see Blumberg *et al.,* 1992).

The parabolic distribution is significant from a biological point of view because the peak turbulent diffusivity occurs at mid-depth in an unstratified water column, and this peak is 1.5 times greater than the depth-averaged diffusivity. Furthermore, in the regions of maximum biological productivity (upper 1 or 2 m in South San Francisco Bay) and in the regions near the bed where the benthic grazing pressure is a maximum, the turbulent diffusivity is relatively small.

b. Effects of stratification. When stratification (gradient zone or pycnocline) is present, the buoyancy force constrains the turbulent eddies, reduces the intensity of the turbulence, and thereby reduces the eddy diffusivity (see, for example, Rodi, 1987; Holt *et al.,* 1992). This effect is local, and the effect of the buoyancy diminishes with distance from the stratified region. For example, in a 10 m water column with stratification (due to salinity or temperature variation) at around 3 or 4 m from the surface, one expects the peak turbulent diffusivity generated by the bottom shear stresses at about 5 m. Although this peak diffusivity is close in value to that at a corresponding point in a similar, unstratified, column the diffusivities above the stratification will be close to molecular values. The resulting turbulent diffusivity distribution has biological relevance because the region of maximum production (euphotic zone) now lies in the zone of minimal mixing.

Ideally, one would solve for the turbulent diffusivities using a time-dependent hydrodynamic simulation of the physical system (e.g., that of Blumberg *et al.,* 1992). Typically, such a simulation involves a turbulent closure model and, thereby, an equation for the turbulent diffusivity as a function of the flow parameters including stratification. It is necessary to solve the time-dependent problem because not only are the flow parameters time-dependent in a estuary, but the mixing action of the turbulence tends to modify the strength of the pycnocline as well as its location.

Because we wished to focus on the transport issues first we chose the more direct and simpler approach of modelling (rather than solving for) the turbulent diffusivity using Eq. (27), and representing the effects of stratification in the "ad-hoc" manner depicted in Figure 1. As shown in Figure 1c we impose a local minimum onto the K profile by multiplying the $K(z)$ function (27) by a stratification function

$$\mathrm{STRAT}(z) = 1 - e^{-(4/w)(z-d)^2}$$

where z is the local depth, w is the depth of the water column affected by the stratification (region of imposed density gradient), and d is the depth from the water surface at which the stratification effect is centered. The distribution shown in Figure 1c, therefore, represents a water column where there is stirring from both the wind at the surface and the tidal currents at the bottom, and where stratification reduces the diffusivity over some region of the water column.

We can further modify this distribution to model the effects of "no wind." In this case the only stirring comes from the bottom stresses, the turbulence will be destroyed by buoyancy in the region of the stratification, and there will be effectively no turbulence above the stratified region. We model this effect by setting the turbulent diffusivity to zero (actually K_0, see Section 2d) at depth d and above (Fig. 1d).

c. Temporal variability of K. The semidiurnal (M_2) tide can generate bottom shear stresses which are comparable in magnitude to the peak spring tide stresses but at a

time scale of hours rather than days. Thus, there are repeated periods of intense mixing on a daily basis which are extremely important to the dynamics of stratification breakdown and, thereby, phytoplankton population dynamics. In order to treat both the M_{sn} and M_2 variation we define the general form of the turbulent mixing coefficient model as

$$K(z, t) = U_*(t)\text{SHAPE}(z) + K_0 \tag{28}$$

where

$$U_*(t) = \kappa H\sqrt{C_d}\,|U(t)|,$$

$$U(t) = u_{\text{avg}} \text{ Sin}\left(\frac{2\pi t}{0.5}\right)\left(1 + 0.5 \text{ Sin}\left(\frac{2\pi t}{14}\right)\right) \qquad (M_2 \text{ and } M_{sn}), \text{ or}$$

$$= u_{\text{avg}}\left(1 + 0.5 \text{ Sin}\left(\frac{2\pi t}{14}\right)\right) \qquad (M_{sn} \text{ only}),$$

$$\text{SHAPE}(z) = \left(\frac{z}{H}\right)\left(1 - \frac{z}{H}\right) \qquad (\text{parabolic } K), \text{ or}$$

$$= 1 \qquad (\text{uniform } K);$$

where K_0 is a small value included for the numerical solution scheme (so that $K(z, t)$ is never equal to zero) (see Section 2b). The magnitude of $U(t)$ using the above formulation is consistent with values published for South San Francisco Bay (see Walters *et al.,* 1985).

Finally, to simulate the breakdown of stratification, we specify the length of time for which the stratification function remains "on" and then a period of time over which the function decays linearly. This is done by multiplying the paramater STRAT(z) by a decay function $D(t)$ such that

$$\text{STRAT}(z, t) = \text{STRAT}(z)D(t). \tag{29}$$

For $u_{\text{avg}} = 0.5$ ms^{-1}, and a parabolic shape function, $K(z, t)$ reaches a maximum of 2510 m^2 d^{-1} at mid-depth. If we average $K(z, t)$ over the depth and the tidal cycle we obtain a $\langle\overline{K}\rangle$ of 530 m^2 d^{-1} which is still one to two orders of magnitude higher than the values used by Cloern (between 5 and 50 m^2 d^{-1}). The primary reason for the difference is that Cloern's values are adjusted to include the effects of stratification and are consistent with what would be calculated (for South San Francisco Bay) from empirical formulae given by Uncles and Joint (1982) for tidally-averaged, stability-dependent, depth-averaged mixing coefficients. The importance of the magnitude of this number and its effect on the results will be discussed later.

Before examining the results of our model it is necessary to discuss some of the issues raised by Gross *et al.* (1992) concerning the validity of eddy diffusivity models based on drag coefficients and shear velocities. In their paper Gross *et al.* state that

such models are inaccurate because they (i) predict zero turbulent diffusivity at slack water, (ii) show the peak diffusivity always to be at the same spatial location, and (iii) do not account for phase shifts that may arise in the distribution of the diffusivity. Their comments are based on simulations done for a 100 m water column. These points are well-taken but we are satisfied that the approach used in this paper is appropriate for the following reasons. First, our simulations are of water columns only 10 m deep, so the turbulence mixing time, H/u_*, is an order of magnitude smaller than for the 100 m case. The water column, therefore, should respond more rapidly to any changes induced by changing tides. Therefore, while the turbulent diffusivity may not be zero at slack water, as predicted by our model, our assumption that the turbulence is exactly in phase with the tidal signal will not produce a large error. Second, the reduced inertia of the 10 m water column (compared to the 100 m case) and the reduced H/u_* means that the shallow water column will respond uniformly to changes in tidal signal. Thus, the phase shifts in the location of the peak diffusivity noted by Gross *et al.* (1992) should not be an issue for the simulations described below.

4. Numerical analysis of the refined 1-d model

In Section 2e we used results from numerical simulations to determine the general conditions necessary for bloom inception in estuaries such as San Francisco Bay. However, these simulations were for conditions of no vertical or temporal variation in K, and no stratification. Here we build on that analysis by examining the conditions necessary for bloom inception when we consider temporal and spatial variation of mixing and the effects of stratification.

a. Scaling revisited. First, we directly extend the analysis in Section 2e for the case of a parabolic distribution of K^* with both M_2 and M_{sn} temporal variation. We performed a similar set of experiments to those summarized in Figure 2 to determine the conditions in which the depth-averaged biomass increases or decreases. The results of these experiments are summarized in Figure 4, which shows that the simulated biomass either increases, decreases, or oscillates about a mean value. In order to plot the results such that Figure 4 could be compared with Fig. 2 (where the turbulent diffusivity is uniform in space and time) we had to choose a representative value of the characteristic turbulent diffusivity, ϵ, to calculate K' (Eq. 27). We used the time-averaged (over a full tidal cycle) value of ϵ at mid-depth, and we define this value to be ϵ_{mean}.

Once again, the regions of behavior in the α'-K' plane are distinct, as shown in Figure 4 for w_s' of 0.37. When $\alpha' = 3.0$ ($\alpha = 4.0$ m d^{-1}) the biomass increases whenever K' is less than 22 ($\epsilon_{mean} < 300$ m^2 d^{-1}), it oscillates whenever K' is between 30 and 37 (ϵ_{mean} between 400 and 500 m^2 d^{-1}), and it decays whenever K' is greater than 44 ($\epsilon_{mean} > 600$ m^2 d^{-1}). The result of Cloern (1991) which showed a bloom is

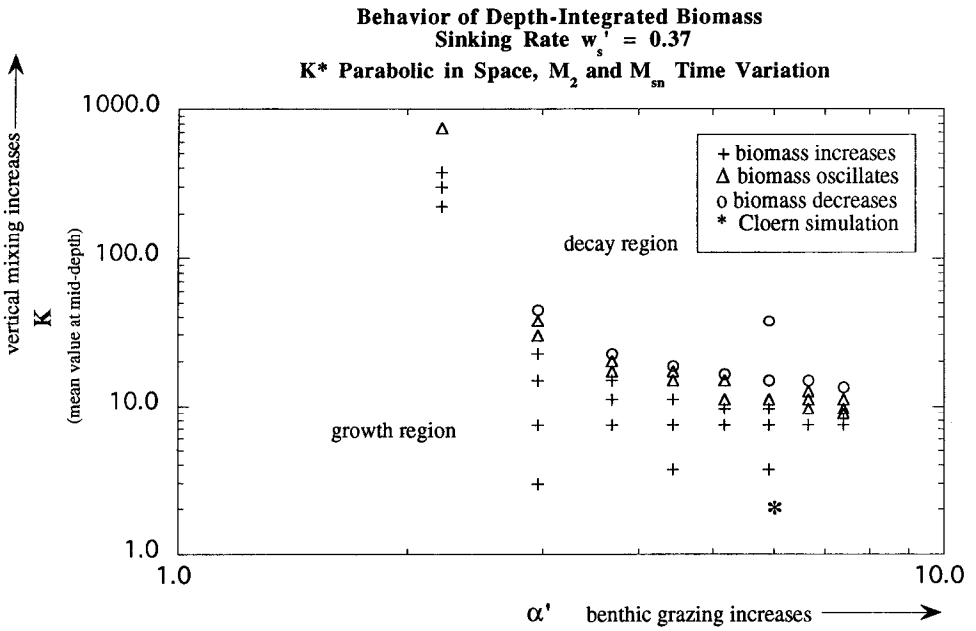

Figure 4. Behavior of depth-integrated biomass as a function of turbulent diffusivity and grazing strength at a fixed value of sinking rate. All variables are non-dimensionalized according to Eqs. (21) to (23), and the turbulent diffusivity distribution is parabolic in space (Fig. 1b) and varies temporally with the M_2 and M_{sn} tides. Curve is dividing line between the growth and decay regions.

also plotted. Cloern used a depth-uniform distribution of K, which varied sinusoidally over a two-week period (M_{sn} tidal simulation). Despite the fact that this distribution tends to overemphasize mixing in the upper regions of the water column where net production is positive, Cloern's model simulated a bloom event by using values for turbulent mixing (5 and 50 $m^2\ d^{-1}$) which are reasonable as depth-averaged values but are unrealistically low as local values. For this particular case $\alpha' = 6.0$ and $K' = 2$, and according to the results presented in Figure 4 this combination of parameters lies in the region of biomass increase. This result is consistent with the results presented in Figure 4 despite the fact that this figure was generated using both M_{sn} and M_2 time-scale variation, whereas Cloern's simulation only used M_{sn}. When, however, the semi-diurnal variation (M_2) was added to the spring-neap variation (α' and K' are still 6 and 2 respectively), the revised model did not produce a bloom of the same magnitude with the same values of turbulent diffusivity K used by Cloern.

Why then is our "theory" not entirely consistent with Cloern's result. The answer probably lies in the fact that the depth-uniform distribution of K tends to overemphasize mixing in the euphotic zone where the net production is positive. (Recall that the values of K' used in Figure 4 are based on a parabolic distribution of turbulent

diffusivity which goes to zero at the water surface.) This effect is minimized when only the M_{sn} variation is considered because there are periods of about 1 to 3 days when K is small ($\sim 5\ m^2\ d^{-1}$) even in the euphotic zone. However, when we add the M_2 timescale these periods may be reduced to 1 to 3 hours! This greatly shortened period of time may not be sufficient for phytoplankton production to have any pronounced effect on biomass before the increased mixing rates redistribute the biomass through the water column. It may be reasonable, then, to hypothesize that the biomass is mixed down and consumed far more rapidly during the periods of intense mixing then it can be produced during the periods of weak mixing.

The difference between our results and those of Cloern's, therefore, underscores the importance of the M_2 tidal variability in estuarine phytoplankton dynamics, as well as that of the spatial distribution of the turbulent diffusivity, especially in the upper regions of the water column where net production is positive. In the following sections, then, we explore the sensitivity of the phytoplankton dynamics to the spatial and temporal variations in turbulent diffusivity. Specifically, we shall concentrate on the interplay between the distribution (in time and space) of the turbulence in the water column, the effect of stratification on this distribution, and the grazing by benthic suspension feeders. We focus first on the role of stratification and turbulent mixing.

b. Role of stratification and wind mixing. From the previous section it is clear that in order to simulate phytoplankton blooms with a realistic distribution of turbulent diffusivity, some physical mechanism must be present to reduce the value of K in the upper region of the water column. There are two necessary conditions leading to reduced mixing in the upper water column. The first is minimal stirring by the wind (see Section 4c). The second is the presence of stratification which (as described above) effectively prevents the turbulence generated at the bed from penetrating into the upper reaches of the water column. Without this stratification, biomass decreases rapidly in simulations run with a benthic grazing rate of $8\ m^3\ m^{-2}\ d^{-1}$ and with a parabolic K which includes M_2 and M_{sn} tidal variation and corresponds to a $0.5\ m\ s^{-1}$ flow velocity.

Our modifications of K to model the effects of stratification are shown in Figure 1. The distribution shown in Figure 1c is representative of a water column with turbulence generated by bottom shear *as well as* wind stirring. A stratification function (see Section 3b) is used to effectively produce a "hole" (region of reduced turbulence) in the parabolic distribution at a level corresponding to the presence of a pycnocline. The stratification function is held constant for six days, with the pycnocline 3 m from the surface, and then allowed to decay linearly during day seven.

However, adding stratification in this manner, with all other parameters the same, again yields a biomass decrease. Figure 5 shows that the depth-averaged biomass for this case and the case of no stratification are nearly identical. To understand the

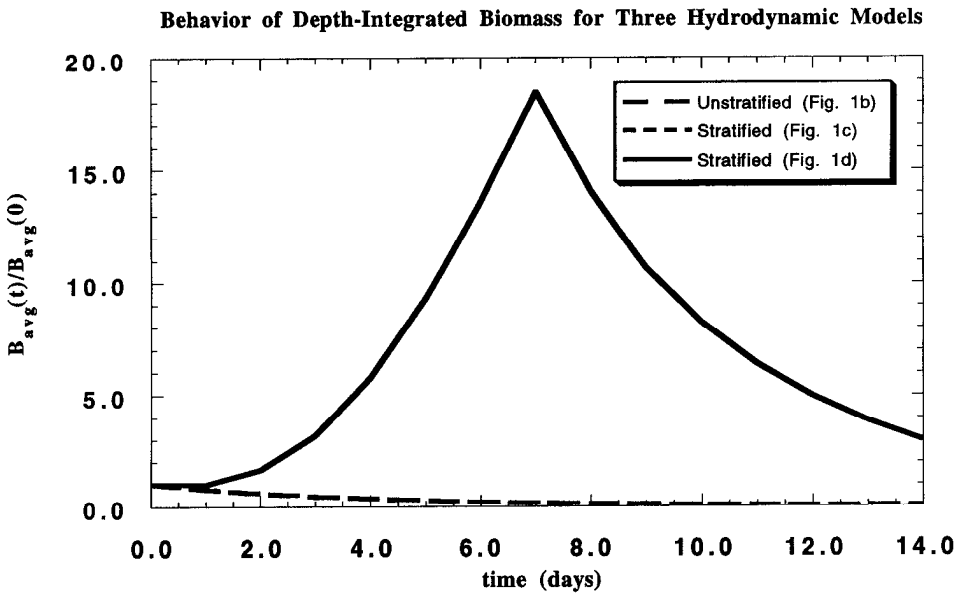

Figure 5. Behavior of depth-integrated biomass for three of the hydrodynamic conditions (b, c, d) shown in Figure 1. The curves for the stratified case (Fig. 1c) and the unstratified case (Fig. 1b) are the same.

interaction between the turbulent diffusion and the biomass concentration we plot, in Figure 6, gray-scale contours of turbulent diffusivity and of biomass as a function of depth and time for two different rates of benthic grazing. The distribution of turbulent diffusivity is shown in Figure 6a and the biomass distribution corresponding to a benthic grazing rate of 8 $m^3\ m^{-2}\ d^{-1}$ which corresponds to α' of 6 is shown in Figure 6b. (The results for a benthic grazing rate of 0 $m^3\ m^{-2}\ d^{-1}$ (α' of 0) shown in Figure 6c are discussed in the next section.) We see in Figure 6b that the biomass decreases at a constant rate with time. Biomass decreases because the values of K in the region of stratification (centered around height of 7 m in Figure 6a) are still high enough that they correspond to K' values in the decay region of the α'-K' plane of Figure 2. As a result, biomass mixes through the stratified zone and is not confined in the photic zone during the period of stratification. We can conclude, therefore, that, even with stratification, as long as wind is stirring the water column a bloom is unlikely.

Next, we modeled the effects of zero wind stirring and stratification by reducing the turbulent diffusivity above the pycnocline to 0 (see Section 3b). The resulting distribution of K is shown qualitatively in Figure 1d. The distribution was derived by taking Eq. (28) with a tidal velocity of 0.5 m s^{-1} and setting the turbulent diffusivity above the pycnocline (z = 3 m) to 0. This distribution would occur if the stratification attenuated the turbulence generated at the lower boundary at the pycnocline, and no

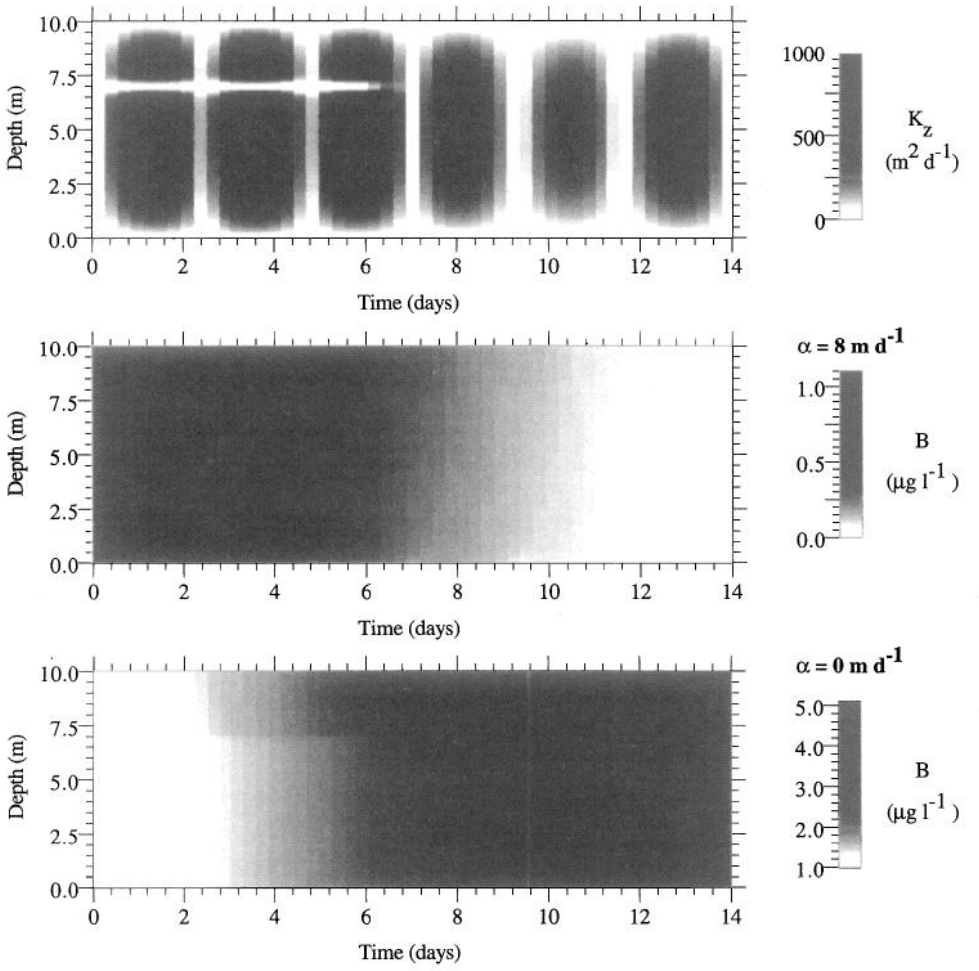

Figure 6. Distribution of turbulent diffusivity (a) and phytoplankton biomass (b, c) as a function of depth and time for two different benthic grazing rates. Turbulent diffusivity distribution is initially specified according to Figure 1c.

wind stirring generated turbulence above the pycnocline. This distribution is actually produced by the turbulence model described by Blumberg *et al.* (1992) when used to simulate tidal flows (see Monismith *et al.,* 1993). This distribution was allowed to persist for 6 days and then "decay" over a period of one day to the case shown in Figure 1b and described in Section 4a.

Figure 5 shows that the depth-averaged biomass increases over the period for which there is zero wind-induced mixing, but it decreases as soon as the turbulent mixing in the upper 3 m of the water column becomes significant. In a similar fashion to the results in Figure 6 we plot, in Figure 7, gray-scale contours of turbulent

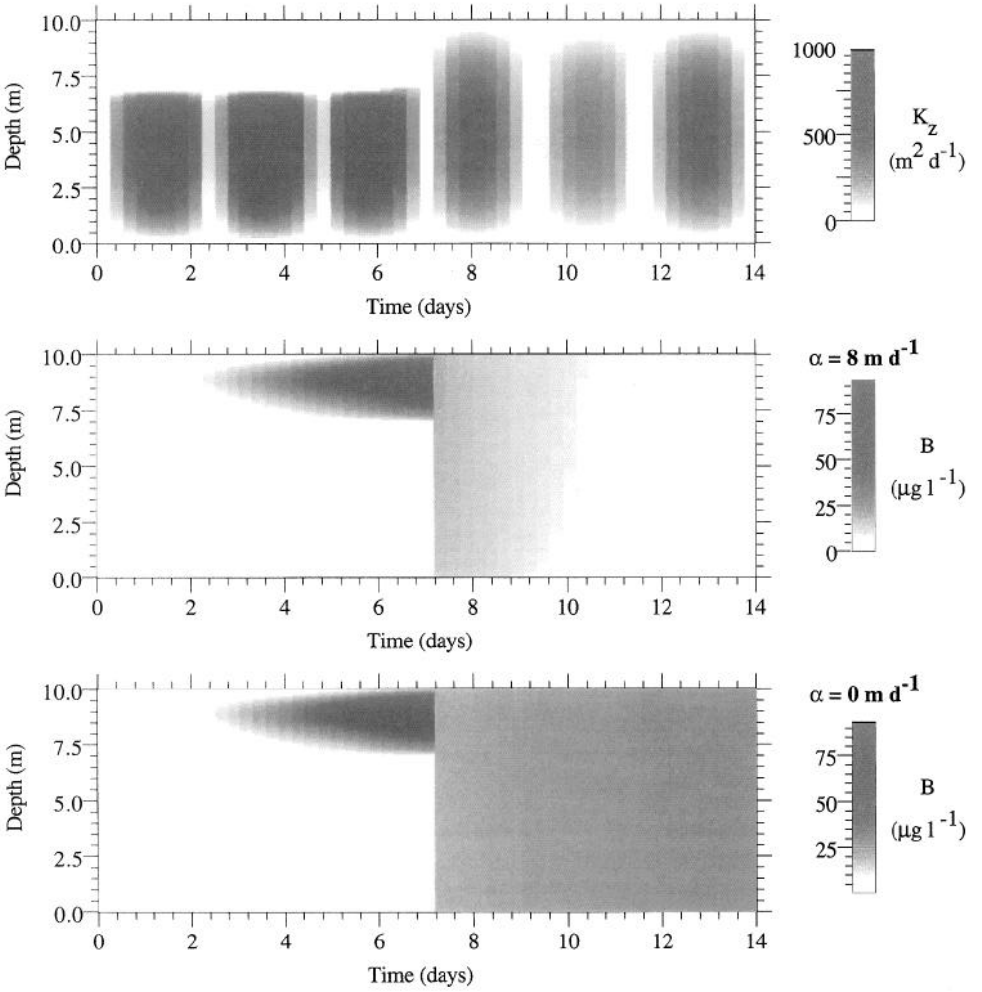

Figure 7. Distribution of turbulent diffusivity (a) and phytoplankton biomass (b, c) as a function of depth and time for two different benthic grazing rates. Turbulent diffusivity distribution is initially specified according to Figure 1d.

diffusivity and biomass as a function of depth and time for the same two values of benthic grazing used in Figure 6. This figure shows that regions of high biomass correspond to regions of low turbulent mixing. The peak concentration at a depth of 1.25 m is a result of the combined effects of sinking and light limitation; sinking reduces the biomass above 1.25 m, while light limitations reduce the production below this level. While this stratification lasts (for six days), reduced mixing above the pycnocline retains phytoplankton in the photic zone so that biomass increases rapidly in the upper layer. However, as soon as the stratification breaks down during day

seven, turbulent mixing (generated at the lower boundary and by wind stirring) rapidly mixes the biomass leading to a nearly uniform distribution, which is then depleted by benthic grazing.

c. Coupling between stratification and benthic grazing. In both Figures 6 and 7 we compare results for two different values of α'. Careful examination of these cases shows that while benthic grazing is an important factor in determining the phytoplankton biomass in the water column, it does not control the occurrence of a bloom. In Figure 6c we see that even with zero benthic grazing the biomass does not increase much above its initial value. Furthermore, in Figure 7c we see that after the stratification breaks down the biomass distribution remains essentially uniform and *does not* increase after day 8. Even though there is no benthic grazing to deplete the water column of biomass, the turbulent mixing is too strong to allow significant biomass increase. It is clear, therefore, that regardless of benthic grazing rate, stratification and minimal wind stirring are both necessary conditions for bloom inception in this model.

5. Some generalities and conclusions

Cloern (1991) showed that hydrodynamic mixing could be a major mechanism controlling the spring phytoplankton bloom in South San Francisco Bay, and in this paper we have further investigated this hypothesis. Scaling analysis of the governing mathematical equations and numerical tests of the behavior of the nondimensional depth-averaged biomass in the α'-K' plane reveal the ranges of α and K values for which biomass can increase or decrease. For a bloom, conditions of mixing and grazing must initially lie in the "growth region," and for the rapid die-off these conditions must then be in the "decay region" of the α'-K' domain.

We investigated several simple models for the turbulent mixing coefficient. Cloern's (1991) model simulated a bloom with a turbulent mixing coefficient having a 14-day period to model the spring-neap tide. We found that the addition of semi-diurnal tidal variation to this model greatly reduces biomass growth, indicating that variations of mixing on the time scale of hours are crucial. In addition, with physically realistic values for the turbulent mixing coefficient this model did not simulate a bloom unless the effects of stratification were included. We found that the only way to simulate a bloom was by including the effects stratification and, further, by prescribing weak mixing in the upper layer.

The results of our numerical experiments indicate that the occurrence of large blooms depends on stratification in two ways. First, stratification is required to confine phytoplankton cells to the photic zone where biomass increase proceeds rapidly. Second, as Cloern hypothesized, stratification removes the connection between benthic grazers and near-surface phytoplankton biomass by decreasing the vertical transport of the biomass. Thus, the occurrence of large blooms is, in general,

a result of stratification providing a favorable light environment, while the eventual disappearance of the biomass is due to benthic grazing coming into play once stratification is eliminated.

Stratification itself is *not* sufficient to ensure that a bloom will develop. Even if the turbulent mixing coefficients are very small in the region of a pycnocline, our model results suggest that mixing rates in the photic zone above the pycnocline must be small to allow significant biomass increase. This result implies that minimal wind stirring is a further prerequisite to bloom development in shallow turbid estuaries, especially those with abundant populations of benthic suspension feeders.

Finally, we wish to clarify our important simplifying assumption that the rate of physiological adjustment to changing light intensity is much slower than the rate at which vertical mixing causes individual cells to sample the complete range of light intensities in the water column (see Section 2c). Assuming first-order kinetics, Lewis *et al.* (1984) show that photoadaptation can be neglected when

$$\Gamma = \frac{K}{L^2\gamma} \gg 1 - e^{-k_s L} \tag{30}$$

where K is the (constant) mixing coefficient, L is the vertical scale over which mixing takes place, γ is the rate constant for photoadaptation, and k_s is the attenuation coefficient for PAR in the water column. Assuming that $k_s L > 1$, this is equivalent to saying that the mixing time-scale must be smaller than the photoadaptation time-scale to neglect photoadaptation.

We can use Lewis *et al.*'s analysis to assess the validity of our assumption of no photoadaptation. For cases without stratification, $L \sim 10$ m, $K_z \sim 1728$ m^2 d^{-1}, and $k_s = 1.3$. For cases with stratification, $L \sim 3$ m and $K_z \sim 1$ m^2 d^{-1} in the upper layer. Cullen and Lewis (1988) show a range of values of γ for a variety of photosynthetic parameters for *Thalassiosira pseudonana*. For example, for $P_{\max}$, they find values of γ ranging from 2×10^{-3} s^{-1} to 1×10^{-4} s^{-1}, depending on the type of adjustment (e.g. high to low intensity) in light involved. If we use an intermediate value of $\gamma = 4 \times 10^{-4}$ s^{-1} we find that for unstratified cases $\Gamma \approx 0.6$, while for stratified cases $\Gamma \approx 0.003$. Thus, because Γ is not $\gg 1$ it is possible that photoadaptation may be important for the conditions of our simulations.

It seems likely that photoadaptation increases production for a given total amount of light, as it would imply that photosynthetic processes in individual cells are operating closer to some optimum level for a given intensity of light. Indeed, attempting to model the effects of light variability in the Neuse estuary by physically cycling incubation bottles through the water column, Mallin and Paerl (1992) found that vertical cycling enhanced productivity by as much as 15% over that found in static incubations. Applied to our model results, Mallin and Paerl's results suggest that photoadaptation would have little effect on biomass production in the presence of grazing, essentially being equivalent to a 15% decrease in grazing, a factor well

within the level of uncertainty of typical estimates of grazing pressure. For cases with stratification and strong blooms, one might hypothesize that photoadaptation might lead to stronger blooms, something that certainly could be investigated by extending the present model along lines similar to those of the phytoplankton model developed by Janowitz and Kamykowski (1991).

Acknowledgments. JRK and SGM wish to acknowledge the support of the US Environmental Protection Agency and the NSF Division of Biological Oceanography through grant numbers CE009605-01-0 and OCE-9102882-01 respectively. JKH was supported by a NASA Fellowship for Global Change Research. The authors wish to acknowledge Graham McBride for reviewing an earlier version of this manuscript, as well as the two anonymous reviewers of this manuscript for their helpful suggestions.

REFERENCES

Bannister, T. T. 1974. A general theory of steady-state phytoplankton growth in a nutrient saturated mixed layer. Limnol. Oceanogr., *19,* 13–30.

Blumberg, A. F., B. Galperin and D. J. O'Connor. 1992. Modeling vertical structure of open-channel flows. J. Hydraulic Eng., *118,* 1119–1134.

Cloern, J. E. 1982. Does the benthos control phytoplankton biomass in South San Francisco Bay (USA)? Mar. Ecol. Progr. Ser., *9,* 191–202.

—— 1987. Turbidity as a control on phytoplankton biomass and productivity in estuaries. Cont. Shelf Res., *7,* 1367–1381.

—— 1991. Tidal stirring and phytoplankton bloom dynamics in an estuary. J. Mar. Res., *49,* 203–221.

Cloern, J. E., T. M. Powell and L. M. Huzzey. 1989. Spatial and temporal variability in South San Francisco Bay. II. Temporal changes in salinity, suspended sediments, and phytoplankton biomass and productivity over tidal time scales. Est. Coast. Shelf Sci., *28,* 599–613.

Cole, B. E. and J. E. Cloern. 1984. Significance of biomass and light availability to phytoplankton productivity in San Francisco Bay. Mar. Ecol. Progr. Ser., *15,* 15–24.

—— 1987. An empirical model of phytoplankton productivity in estuaries. Mar. Ecol. Progr. Ser., *36,* 299–305.

Colijn, F. 1982. Light absorption in the waters of the Ems-Dollard estuary and its consequences for the growth of phytoplankton and microphytobenthos. Neth. J. Sea Res., *15,* 196–216.

Cullen, J. J. and M. R. Lewis. 1988. The kinetics of algal photoadaptation in the context of vertical mixing. J. Plankton Res., *10,* 1039–1063.

Evans, G. T. and J. S. Parslow. 1985. A model of annual plankton cycles. Biol. Oceanogr., *3,* 327–347.

Fischer, H. B., E. J. List, R. C. Y. Koh, J. Imberger and N. H. Brooks. 1979. Mixing in Inland and Coastal Waters. Academic Press, New York, 106 pp.

Fortier, L. and L. Legendre. 1979. Le contrôle de la variabilité á courte terme du phytoplancton estuarien: stabilité verticale et profondeur critique. J. Fish. Res. Board Can., *36,* 1325–1335.

Gieskes, W. W. C. and G. W. Kraay. 1975. The phytoplankton spring bloom in Dutch coastal waters of the North Sea. Neth. J. Sea Res., *9,* 166–196.

Gran, H. H. and T. Braarud. 1935. A quantitative study on the phytoplankton of the Bay of Fundy and the Gulf of Maine including observations on hydrography, chemistry and morbidity. J. Biol. Bd. Can., *1,* 219–467.

Greenspan, D. and V. Casulli. 1988. Numerical Analysis for Applied Mathematics, Science, and Engineering. Addison-Wesley Publishing Company, Redwood City, California.

Gross, T. F., F. E. Werner and J. E. Eckman. 1992. Numerical modeling of larval settlement in turbulent bottom boundary layers. J. Mar. Res., *50,* 611–642.

Hitchcock, G. L. and T. J. Smayda. 1977. The importance of light in the initiation of the 1972–1973 winter-spring diatom bloom in Narragansett Bay. Limnol. Oceanogr., *22,* 126–131.

Holt, S. E., J. R. Koseff and J. H. Ferziger. 1992. A numerical study of the evolution and structure of homogeneous stably stratified sheared turbulence. J. Fluid Mech., *237,* 499–539.

Janowitz, G. S. and D. Kamykowski. 1991. An Eulerian model of phytoplankton photosynthetic response in the upper mixed layer. J. Plankton Res., *13,* 983–1002.

Jassby, A. D. and T. Platt. 1976. Mathematical formulation of the relationship between photosynthesis and light for phytoplankton. Limnol. Oceanogr., *21,* 540–547.

Kemp, W. M. and W. R. Boynton. 1984. Spatial and temporal coupling of nutrient inputs to estuarine primary production: the role of particulate transport and decomposition. Bull. Mar. Sci., *35,* 522–535.

Lewis, M. R., J. J. Cullen, and T. Platt. 1984. Relationships between vertical mixing and photoadaptation of phytoplankton: similarity criteria. Mar. Ecol. Prog. Ser., *15,* 141–149.

Lyne, V. D. 1983. 1983. The role of hydrodynamic processes in planktonic productivity. Report ED-83-035, Dept. of Civil Eng., Univ. of Western Australia, Nedlands, Western Australia.

Mallin, M. A. and H. W. Paerl. 1992. Effects of variable irradiance on phytoplankton productivity in estuaries. Limnol. Oceanor., *37,* 54–62.

Malone, T. C. 1992. Effects of water column processes on dissolved oxygen, nutrients, phytoplankton and zooplankton, *in* Oxygen Dynamics in the Chesapeake Bay, A Synthesis of Research, D. E. Smith, M. Leffler and G. Mackiernan, eds., Maryland Sea Grant, College Park, Maryland, 61–112.

Monismith, S. G., D. Fong and M. Stacey. 1993. Simple model of vertical mixing in a stratified tidal flow (in preparation).

Nixon, S. W. 1981. Remineralization and nutrient cycling in coastal marine ecosystems, *in* Estuaries and Nutrients, B. J. Neilson and L. E. Cronin, eds., Humana Press, Clifton, New Jersey, 111–138.

Platt, T., D. F. Bird and S. Sathyendranath. 1991. Critical depth and marine primary production. Proc. R. Soc. Lond. B, *246,* 205–217.

Riley, G. A. 1942. The relationship of vertical turbulence and spring diatom flowerings. J. Mar. Res., *5,* 67–87.

Rodi, W. 1987. Examples of calculation methods for flow and mixing in stratified fluids. J. Geophys. Res., *92,* C5, 5305–5328.

Sellner, K. G., R. V. Lacouture, S. J. Cibik, A. Brindley and S. G. Brownlee. 1991. Importance of a winter dinoflagellate-microflagellate bloom in the Patuxent River estuary. Est. Coast. Shelf Sci., *32,* 27–42.

Simpson, J. H., J. Brown, J. Matthews and G. Allen. 1990. Tidal straining, density currents, and stirring in the control of estuarine stratification. Estuaries, *13,* 125–132.

Simpson, J. H., J. Sharples and T. P. Rippeth. 1991. A prescriptive model of stratification induced by freshwater runoff. Est. Coast. Shelf Sci., *33,* 23–35.

Sinclair, M., D. V. Subba Rao and R. Couture. 1981. Phytoplankton temporal distribution in estuaries. Oceanol. Acta, *4,* 239–246.

Smayda, T. J. 1989. Primary production and the global epidemic of phytoplankton blooms in the sea: a linkage?, *in* Novel Phytoplankton Blooms, E. M. Cosper, V. M. Bricelj and E. J. Carpenter, eds., Springer-Verlag, New York, 449–484.

Sverdrup, H. U. 1953. On conditions for vernal blooming of phytoplankton. J. Cons. Perm. Int. Explor. Mer., *18,* 287–295.

Taylor, G. I. 1954. The dispersion of matter in turbulent flow through a pipe. Proc. R. Soc. London Ser. A223, 446–448.

Uncles, R. J. and I. R. Joint. 1982. Vertical mixing and its effect on phytoplankton growth in a turbid estuary. Canadian J. Fisheries and Aquatic Sci., *40,* 221–228.

Walters, R. A., R. T. Cheng and T. J. Conomos. 1985. Time scales of circulation and mixing processes of San Francisco Bay Waters, *in* Temporal Dynamics of an Estuary: San Francisco Bay, J. E. Cloern and F. H. Nichols, eds., Dr. W. Junk Publishers, Dordrecht, 13–36.

Wienke, S. M. and J. E. Cloern. 1987. The phytoplankton component of seston in San Francisco Bay. Neth. J. Sea Res., *21,* 25–33.

Winter, D. F., K. Banse and G. C. Anderson. 1975. The dynamics of phytoplankton blooms in Puget Sound, a fjord in the northwestern United States. Mar. Biol., *29,* 139–176.

Wroblewski, J. S. 1989. A model of the spring bloom in the North Atlantic and its impact on ocean optics. Limnol. Oceanogr., *34,* 1563–1571.

Received: *20 April, 1993;* Revised: *30 June, 1993.*